Modulation of Extrinsic and Intrinsic Signaling Together with Neuronal Activation Enhances Forelimb Motor Recovery after Cervical Spinal Cord Injury

Hirohide Takatani,[1,2] Naoki Fujita,[2] Fumiyasu Imai,[1,3] and Yutaka Yoshida[1,3,4]

[1]Neural Connectivity Development in Physiology and Disease Laboratory, Burke Neurological Institute, White Plains, New York 10605, [2]Laboratory of Veterinary Surgery, Graduate School of Agriculture and Life Sciences, The University of Tokyo, Bunkyo-ku, Tokyo 113-0032, Japan, [3]Brain and Mind Research Institute, Weill Cornell Medicine, New York 10065, and [4]Neural Circuit Unit, Okinawa Institute of Science and Technology Graduate University, Onna-son, Kunigami-gun, Okinawa 904-0495, Japan

Abstract

Singular strategies for promoting axon regeneration and motor recovery after spinal cord injury (SCI) have been attempted with limited success. For instance, the deletion of *RhoA* and phosphatase and tensin homolog (*Pten*) (an extrinsic and intrinsic modulating factor, respectively) in corticospinal neurons (CSNs) promotes axon sprouting after thoracic SCI; however, it is unable to restore motor function. Here, we examine the effects of combining *RhoA/Pten* deletion in CSNs with chemogenetic neuronal stimulation on axonal growth and motor recovery after SCI in mice. We find that this combinatorial approach promotes greater axonal growth and presynaptic bouton formation in CSNs within the spinal cord compared with *RhoA*;*Pten* deletion alone. Furthermore, chemogenetic neuronal stimulation of *RhoA*;*Pten*-deleted CSNs improves forelimb performance in behavioral tasks after SCI compared with *RhoA*;*Pten* deletion alone. These results demonstrate that combination therapies pairing genetic modifications with neuronal stimulation can promote greater presynaptic formation and motor recovery following SCI than either strategy alone.

Key words: corticospinal tract; hM3Dq; Pten; RhoA; spinal cord injury

Significance Statement

In this study, we examined whether pairing neural stimulation with genetic deletion of *RhoA* and *Pten* in corticospinal neurons (CSNs) would enhance axonal growth and motor recovery after spinal cord injury (SCI). We found that this combinatorial approach, relative to singular strategies, promoted greater presynaptic bouton formation in injured CSNs in the spinal cord, resulting in improved motor recovery in those mice. These results open the possibility for even greater enhancements in healing and recovery following SCI through carefully crafted, multifaceted treatments tailored to address the specific needs of individual SCI patients.

Introduction

Recovery of motor function after spinal cord injury (SCI) is likely to require substantial axonal growth and neural rewiring. In the adult central nervous system, full recovery from SCI is rarely observed. The corticospinal tract (CST), the major descending tract that controls voluntary movements, conveys motor commands from the sensorimotor cortex to the spinal cord, making it an important target for axon regeneration following SCI (Porter and Lemon, 1993; Oudega and Perez, 2012; Nicola et al., 2022). Although

numerous potential therapeutic methods have been attempted, no single approach has fully reconstructed the injured CST or restored motor function after SCI. We propose that a combinatorial strategy targeting signaling pathways and neural activity may yield superior results compared with individual therapies.

Several molecules, such as phosphatase and tensin homolog (Pten), KLF7, Rho, and Sox11, have been shown to prevent axon regeneration after SCI (Liu et al., 2010; Blackmore et al., 2012; Fujita and Yamashita, 2014; Wang et al., 2015). Pten is an enzyme that suppresses the mechanistic target of rapamycin (a critical signaling component for axon growth), which prevents new protein synthesis and neuronal growth (Zhang et al., 2018). Deletion of *Pten* promotes significant regeneration of corticospinal (CS) axons after SCI, facilitating robust extension of axons across the lesion site (Liu et al., 2010). In addition, the Rho family of small GTPases, including RhoA, are important regulatory signaling molecules that are triggered by extrinsic molecules, such as myelin-associated inhibitors, repulsive axon guidance molecules, and inhibitory extracellular matrix molecules after SCI (Fujita and Yamashita, 2014). The Rho signaling pathway is involved in actin cytoskeletal dynamics that can lead to growth cone collapse and axon growth inhibition. Pharmacological Rho inhibitors enhance sprouting and regeneration of CS axons after SCI, but the extent of regeneration is variable (Fournier et al., 2003; Duffy et al., 2009; Boato et al., 2010; Fujita and Yamashita, 2014). It has already been shown that co-deletion of *RhoA* and *Pten* from the sensorimotor cortex prior to SCI resulted in reduced CS axonal dieback and enhanced rewiring of CS circuits to the spinal cord and hindlimb muscles; however, this approach to changing the internal growth state of CS neurons (CSNs) alone did not promote axon regrowth through the lesion and did not enhance hindlimb motor recovery after SCI (Nakamura et al., 2021). A method for eliciting and strengthening novel CS circuits may be required for capitalizing on the enhanced axonal plasticity resulting from *RhoA* and *Pten* deletion.

Neuronal stimulation is a robust approach for driving CS circuit plasticity that may promote motor recovery. Previous studies indicate that electrical stimulation of the cortex can transform neuronal circuits from a nonfunctional to a highly functional state and promote extensive sprouting of CSNs which restores neurological function after SCI (Carmel and Martin, 2014; Squair et al., 2021). Moreover, activation of the sensorimotor cortex by excitatory designer receptors exclusively activated only by designer drugs (DREADDs) promotes CS axon growth and increases their projections to the spinal cord (Yang and Martin, 2023). In another study, chemogenetic stimulation of spinal neurons using DREADDs induced axon sprouting and restored locomotion after SCI by administering actuator ligands (Brommer et al., 2021). In addition, such chemogenetic stimulation of CSNs in both supraspinal centers and spinal relay stations results in enhancement of neuronal rewiring and locomotor recovery (Van Steenbergen et al., 2023). Together, neuronal stimulation of the *RhoA;Pten*-deleted axons, which have regained the potential to grow and sprout, might be a novel strategy to enhance axon regeneration and motor recovery after SCI.

In this study, we determined whether combining *RhoA;Pten* deletion in CSNs with chemogenetic neuronal stimulation synergistically enhances CS circuit rewiring and forelimb functional recovery after cervical SCI in mice. Our results demonstrate that this combinatorial intervention spurred CS axon regrowth. Additionally, such intervention achieved partial restoration of forelimb motor recovery. Our results, therefore, strongly suggest that combinatorial treatment strategies, specifically tailored to the needs of individual patients, will maximize motor recovery in those impacted by traumatic SCI.

Materials and Methods

Animals

RhoA^{f/f} (Chauhan et al., 2011; Katayama et al., 2011; Melendez et al., 2011) and *Pten^{f/f}* (The Jackson laboratory; Lesche et al., 2002) mice were crossed to create *RhoA^{f/f};Pten^{f/f}* mice that were maintained on a C57BL/6 background. Males and females were used in the experiments. Mice were isolated in individual cages in a pathogen-free environment under a 12 h light/dark cycle and fed commercial pellets and water *ad libitum*.

Ethics declaration

Procedures were performed in accordance with protocols approved by the Weill Cornell Medicine Institutional Animal Care and Use Committee. All experiments were performed in a manner that minimized pain and discomfort of the mice.

Correspondence should be addressed to Yutaka Yoshida at yoy4001@med.cornell.edu.

Adeno-associated viruses (AAVs)

The following AAVs were used in experiments: AAV8-Ef1a-fDIO-Cre (AAV8-fDIO-Cre; 2.1×10^{13} GC/ml, Addgene, 121675-AAV8; Schneeberger et al., 2019), AAV8-Ef1a-fDIO-mCherry (AAV8-fDIO-mCherry; 1.8×10^{13} GC/ml, Addgene, 114471-AAV8), AAV8-CMV-LacZ (AAV8-LacZ; 1.7×10^{13} GC/ml, Addgene, 105531-AAV8), AAV1-hsyn-Cre (AAV1-Cre; 1.9×10^{13} GC/ml, Addgene, 105553-AAV1), AAV1-hsyn-GFP (AAV1-GFP; 1.0×10^{12} GC/ml, Addgene, 50465-AAV1), AAVretro-Ef1a-Flpo (AAVretro-Flpo; 1.6×10^{13} GC/ml, Addgene, 55637-AAVrg; Fenno et al., 2014), and AAVretro-hsyn-DIO-hM3Dq-mCherry (AAVretro-DIO-hM3Dq-mCherry; 1.9×10^{13} GC/ml, Addgene, 44361-AAVrg; Krashes et al., 2011).

Surgeries

AAV injections. Mice were anesthetized with isoflurane and placed in a stereotaxic frame (Stoelting, 51730D). For brain injections, the scalp was incised (incision size of 10×10 mm^2), and holes were made in the skull at the corresponding AAV injection sites using a round stainless-steel drill (⌀ 0.5 mm). AAVs were injected into the rostral forelimb and caudal forelimb areas (RFA and CFA, respectively) of the sensorimotor cortex [depth of 0.5 mm; coordinates, 1.8 mm anterior, 1.2 mm lateral to the bregma, 0.6 mm posterior, 1.8 mm lateral to the bregma (Wang et al., 2017), 0.2 µl/virus/site] using a Nanoject III injector (Drummond Scientific Company, 3-000-207) tipped with a glass micropipette. For spinal cord AAV injections, skin and muscles on the cervical region of the neck were incised, exposing the C4 vertebrae. AAVs were injected into the C5 region of the spinal cord (depth of 0.5 mm and 1.0 mm; coordinates, 0.5 mm anterior, 0.5 mm lateral to the center of C4 vertebrae, 0.5 mm posterior, 0.5 mm lateral to the center of C4 vertebrae, 0.15 µl/virus/site) using the Nanoject III instrument.

Spinal cord injury (SCI). Dorsal column lesions were made as previously described (Hollis et al., 2016). Briefly, after anesthetization with isoflurane, a laminectomy at the C4 vertebrae was performed to expose the spinal cord. A dorsal column lesion (depth of 1.0 mm) was made at the C5 vertebrae using Vannas spring scissors (2.5 mm cutting edge) to sever the dorsal CST.

Analgesia. Prior to skin incision, 100 µl of a mixture of 2% lidocaine and 0.5% bupivacaine was administered subcutaneously as a local analgesic. Buprenorphine (0.5 mg/kg) was administered subcutaneously as a postoperative analgesic immediately following surgery and twice per day thereafter for 3 d. Meloxicam (0.2 mg/kg) was additionally administered subcutaneously following AAV injections. Syringes equipped with 30 G needles were used for all injections.

Western blots

Dissected brains were sectioned using a mouse coronal brain slicer (Kent Scientific, rbma-200c). Areas of the brain in which GFP fluorescence was detected were collected and homogenized in lysis buffer [50 mM Tris-HCl, pH 8.0, containing 150 mM NaCl, 1% NP-40, 0.5% sodium deoxycholate, 0.1% SDS, and protease inhibitor cocktail (Abcam, ab271306)]. After centrifugation at $10,000 \times g$ for 10 min at 4°C, the protein concentration was adjusted to 1 mg/ml. Proteins were separated by SDS-PAGE and transferred to a PVDF membrane (Bio-Rad, 162-0177). Chameleon NIR Duo-Prestained Protein Ladder (LICORbio, 928-60000) was used to estimate protein band sizes. The PVDF membrane was blocked with 5% skim milk in PBS containing 0.05% Tween 20 and then incubated overnight at 4°C with either rabbit anti-RhoA (1:1,000, Cell Signaling Technology, 67B9), rabbit anti-Pten (1:1,000, Cell Signaling Technology, 9188S), or mouse Tuj1 (1:1,000, BioLegend, MMS-435P). After washing, the membrane was incubated with anti-rabbit IRDye 680RD (LI-COR, 925-68072) and anti-mouse IRDye 800 (LI-COR, 925-32213). An Odyssey Clx Imager (LI-COR) was used to detect and quantify antibody-bound proteins.

Histology

Dissected brains and spinal cords were postfixed in 4% PFA overnight. The tissues were then cryopreserved at 4°C in 30% sucrose/PBS overnight and then embedded in a Tissue-Tek optimal cutting temperature compound (Sakura Finetek). Embedded samples were sliced using a cryostat into 50-µm-thick sections and floated on PBS. The sections were then blocked with 1% bovine serum albumin/PBS for 1 h before incubating at 4°C overnight with rat anti-glial fibrillary acidic protein (GFAP; Thermo Fisher Scientific, 13-0300), rabbit anti-cFos (Cell Signaling Technology, 2250S), rabbit anti-PKCγ (Abcam, ab71558), or rat anti-myelin basic protein (MBP; Abcam, ab7349) antibodies. After washing with 0.1% Tween 20/PBS (PBS-t), the sections were incubated with Alexa Fluor 488 anti-rat (Invitrogen, A21208), Alexa Fluor 488 anti-rabbit IgG antibodies (Invitrogen, A21206), or Alexa Fluor 647 anti-rabbit IgG antibodies (Invitrogen, A31573). The sections were then washed with PBS and mounted onto glass slides (Fisherbrand, 1255015). Sections were counterstained with DAPI (1 µg/ml, Invitrogen, D1306) and washed with PBS-t, and 200 µl of mounting media (VectorLabs, H10000-10) was applied directly onto the sections before covering with coverslips (VWR, 48393-251). The slide-mounted sections were scanned using a confocal microscope (Nikon A1R HD25).

Quantification of activated CSNs

To quantify cFos expression as a marker of neural activity in CSNs (Fig. 3), coronal sections of the brain that exhibited mCherry$^+$ CSNs were selected (5–7 sections per sample). Using ImageJ software, mCherry$^+$ CSNs were detected and counted in the confocal 16 bit red channel image. The intensity of cFos (fluorescently stained with Alexa Fluor 488) within

the mCherry$^+$ CSNs was then detected in the 16 bit green channel image and the cFos$^+$ neurons were counted. The percentage of cFos$^+$ CSNs was calculated by dividing the cFos$^+$/mCherry$^+$ CSNs by the total number of mCherry$^+$ CSNs.

Quantification of CST dieback

CST dieback analysis was carried out following established quantification methods with some modifications (Nakamura et al., 2021). To quantify the dieback and regeneration of CST axons, 3–5 sagittal sections of the spinal cord that included the mCherry$^+$ CST axons were chosen in each sample, and the mCherry intensities within the CST fibers in the dorsal column were measured by ImageJ software. The center of the lesion was set as 0 μm, and measurements were taken at 100 μm intervals along the rostral–caudal axis (Extended Data Fig. 4-1). Each region of interest was set to a width of 100 μm and a height of 500 μm. To normalize the differences between individual animals, the mCherry intensity in each distance bin was divided by the intensity of mCherry in the rostral 1,000 μm bin (−1,000 μm from the lesion), and this value was defined as the axon index. To assess the suppression of axon dieback relative to control mice, the mCherry axon indices of the *RhoA;Pten* double conditional KO (dcKO) mice and the dcKO with DREADD (dcKO$^{hM3Dq\ and\ water}$ and dcKO$^{hM3Dq\ and\ DCZ}$) mice were divided by the mean index of the control mice (LacZ and LacZ^{DCZ}), and this calculated value was defined as the mCherry axon index ratio.

Quantification of axon collateral projections

Axon collateral projection analysis was carried out following established quantification methods with some modifications (Nakamura et al., 2021). Transverse sections of the spinal cord at 0, 50, 100, 150, and 200 μm rostral, and 50 and 100 μm caudal, to the lesion were chosen to quantify axon collaterals (Fig. 6). To determine the center of the lesion, consecutive sections that likely included the lesion were first identified and the middlemost section was set as the center. The mCherry intensity of CST fibers in the gray matter was measured in each section by ImageJ software. As in prior experiments, the mCherry intensity in the dorsal funiculus at 1,000 μm rostral to the lesion was used for normalization, since axon dieback is limited at this distance and reflects the full transduction of CST neurons. This normalized value was defined as the mCherry axon collateral index (Fig. 6c,d).

Quantification of presynaptic boutons

The total number of mCherry$^+$ boutons was quantified by Imaris AI microscopy image analysis software. Boutons with diameters greater than 5 μm were selected and counted from transverse sections of the spinal cord at 0, 50, 100, 150, and 200 μm rostral, and 50 and 100 μm caudal, to the lesion site. The number of boutons was normalized by dividing by the mCherry intensity in the dorsal funiculus 1,000 μm rostral to the lesion. This normalized value was defined as the bouton index (Fig. 6f).

Behavioral analyses

A grid-walking test using an elevated square wire grid (20 × 20 cm^2 with 1.2 × 1.2 cm^2 grid cells) was used to evaluate the effects of SCI on the skilled behaviors of treated and control mice. A custom-made transparent acrylic tube (25 cm diameter) was placed over the grid to prevent mice from walking on the grid's outer edges. Limb slips were detected during playbacks of video recordings (30 frames/s) of traversal attempts. A mirror was placed under the grid at an angle of 45°, and the reflection was recorded with another video camera to identify the limbs that slipped from the grid.

Mice were subjected to the grid-walking test prior to SCI (preinjury) and then again at 7, 14, 21, 28, 35, 42, and 49 d postinjury (DPI). Mice were allowed to walk on the grid for 3 min, and foot-slips of the left and right forelimbs were counted during the first 50 forelimb steps. A slip was scored when the forepaw completely missed the grid and the limb fell between the wires, or when the forepaw was correctly placed on the grid but slipped off during the weight-bearing phase (Chao et al., 2012). The percentage of slips was calculated as the number of slips divided by the first 50 steps per trial × 100. To normalize the differences between animals, the slip rate at each DPI was divided by the preinjury rate, and this value was defined as the slip rate index. To show performance deterioration relative to controls, the slip rate indices of mice with *RhoA;Pten* deletion in CSNs (dcKO) and dcKO with DREADD mice (dcKO$^{hM3Dq\ and\ water}$ and dcKO$^{hM3Dq\ and\ DCZ}$) were divided by the mean index of the control mice (LacZ and LacZ^{DCZ}), and this value was defined as the slip rate index ratio.

Evaluation and statistical analyses

Mice were randomly chosen from a *RhoA$^{f/f}$;Pten$^{f/f}$* mouse population and divided into cohorts for AAV injections prior to SCI. The mice were then randomly assigned numbers for the grid-walking task, which was conducted in a blinded manner.

Statistical analyses were performed using R software with all quantitative data represented as the standard error of the mean. Differences among groups were statistically analyzed using a two-tailed unpaired *t* test, Wilcoxon rank sum exact test, two-way ANOVA followed by Tukey's test, or Kruskal–Wallis test followed by Wilcoxon rank sum exact test. A *p*-value of <0.05 was considered statistically significant.

Experimental design

To delete *RhoA* and *Pten* in CSNs, 6-week-old *RhoA$^{f/f}$;Pten$^{f/f}$* mice were injected with AAV1-GFP or AAV1-Cre in the RFA and CFA of the sensorimotor cortex (Fig. 1a). Two weeks later, animals were killed by CO_2 exposure, and brains were dissected and processed for Western blotting.
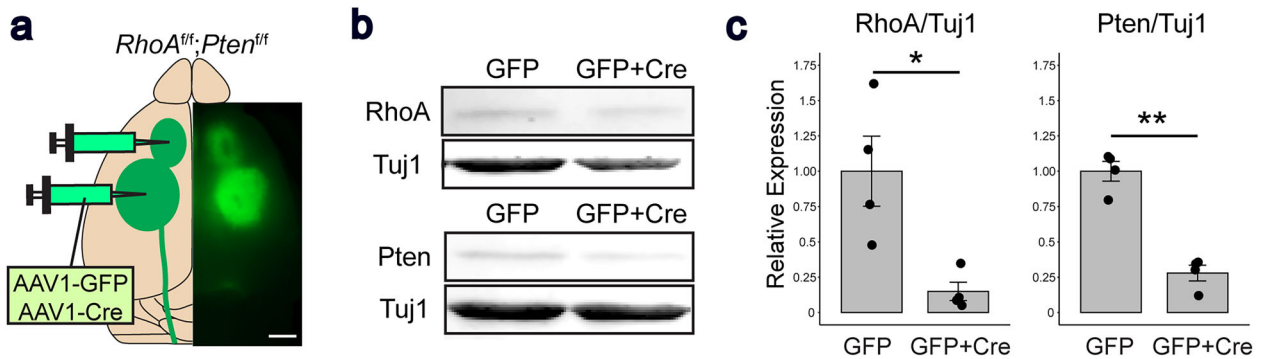
Figure 1. Genetic deletion of *RhoA* and *Pten* in the sensorimotor cortex. ***a***, Schematic illustration showing the AAV1-Cre-mediated gene deletion strategy. AAV1-GFP and AAV1-Cre (GFP + Cre) were injected into the RFA and CFA, respectively, in the brains of *RhoA^{f/f};Pten^{f/f}* mice. The stereomicroscopic image shows GFP expression in the cerebral cortex (right panel). Scale bar, 2 mm. ***b***, ***c***, Western blot analysis of RhoA (21 kDa) and Pten (54 kDa) in the cerebral cortex of AAV-injected *RhoA^{f/f};Pten^{f/f}* mice. Tuj1 (55 kDa) was used as a loading control. The relative band intensities of RhoA and Pten, normalized to Tuj1, were significantly reduced in the GFP + Cre coinjected mice. ***c***, Full Western blot images are shown in Extended Data Figure 1-1. Unpaired *t* test (GFP; $n = 4$, GFP + Cre; $n = 4$). *$p < 0.05$, **$p < 0.005$. Specific data is in Table 1.

Dorsal column transections were performed to completely sever the CSTs of mice (Extended Data Fig. 2-2). The effectiveness of the procedure was assessed by euthanizing *RhoA^{f/f};Pten^{f/f}* mice 2 weeks after transection and examining their spinal cord tissues after immunohistochemical (IHC) processing. MBP antibodies were used to evaluate whether the dorsal column had been fully severed, and protein kinase C gamma (PKCγ) antibodies, which specifically bind to active CSNs, were used to evaluate whether the CST was transected by the lesion.

To assess the levels of axon dieback and the impacts on forelimb motor behavior following *RhoA;Pten* deletion and neuronal activation using excitatory DREADDs, 6–8-week-old *RhoA^{f/f};Pten^{f/f}* mice were injected with various combinations of AAVs. Intracortical injections of AAV8 infects all or most of the forelimb-related CST tissues anterogradely, while injection of AAVretro into the C5 spinal cord infects the CST and other descending spinal tracts retrogradely (Fig. 2a). By combining the cortical injection of an AAV8 vector encoding a recombinase-dependent gene of interest, with a C5 spinal cord injection of an AAVretro vector providing the needed recombinase, we can express the gene of interest in CSNs projecting to the spinal cord including the C5 level (Fig. 2a).

Five mouse cohorts were prepared for this study (Fig. 2b):

1. LacZ
   AAV8-LacZ and AAV8-fDIO-mCherry were injected into the sensorimotor cortex, while AAVretro-Flpo was injected into the C5 spinal cord of *RhoA^{f/f};Pten^{f/f}* mice. In this cohort, mCherry will be expressed in CSNs projecting to the C5 spinal cord.
2. LacZ^{DCZ}
   AAV8-LacZ and AAV8-fDIO-mCherry were injected into the sensorimotor cortex, while AAVretro-Flpo and AAV8-DIO-hM3Dq-mCherry were injected into the cervical spinal cord of *RhoA^{f/f};Pten^{f/f}* mice. This cohort will express mCherry in CSNs projecting to the C5 spinal cord. The DREADD agonist, deschloroclozapine (DCZ; MCE, HY-42110), was intraperitoneally (i.p.) injected after the SCI.
3. Double conditional knock out (dcKO)
   AAV8-fDIO-Cre and AAV8-fDIO-mCherry were injected into the sensorimotor cortex, and AAVretro-Flpo was injected into the cervical spinal cord of *RhoA^{f/f};Pten^{f/f}* mice. In this cohort, *RhoA;Pten* are deleted and mCherry will be expressed in CSNs projecting to the C5 spinal cord.
4. Double conditional knock out with hM3Dq with administration of water (dcKO^{hM3Dq and water})
   AAV8-fDIO-Cre and AAV8-fDIO-mCherry were injected into the sensorimotor cortex, and AAVretro-Flpo and AAV8-DIO-hM3Dq-mCherry were injected into the cervical spinal cords of *RhoA^{f/f};Pten^{f/f}* mice. *RhoA;Pten* are deleted in this cohort, and hM3Dq and mCherry will be expressed in CSNs projecting to the C5 spinal cord. Water was i.p. injected after the SCI.
5. Double conditional knock out with hM3Dq with administration of DCZ (dcKO^{hM3Dq and DCZ})
   AAV8-fDIO-Cre and AAV8-fDIO-mCherry were injected into the sensorimotor cortex, and AAVretro-Flpo and AAV8-DIO-hM3Dq-mCherry were injected into the cervical spinal cords of *RhoA^{f/f};Pten^{f/f}* mice. In this cohort, *RhoA;Pten* are deleted, and hM3Dq and mCherry will be expressed in CSNs projecting to the C5 spinal cord. DCZ was i.p. injected after SCI.

The LacZ and LacZ^{DCZ} groups were prepared as control groups in which *RhoA;Pten* are not deleted and excitatory DREADD is not expressed in the CST due to the lack of Cre (Fig. 2b). The dcKO group only expresses the conditional KO (Fig. 2b). The dcKO^{hM3Dq and water} and dcKO^{hM3Dq and DCZ} groups both express the conditional KO with excitatory
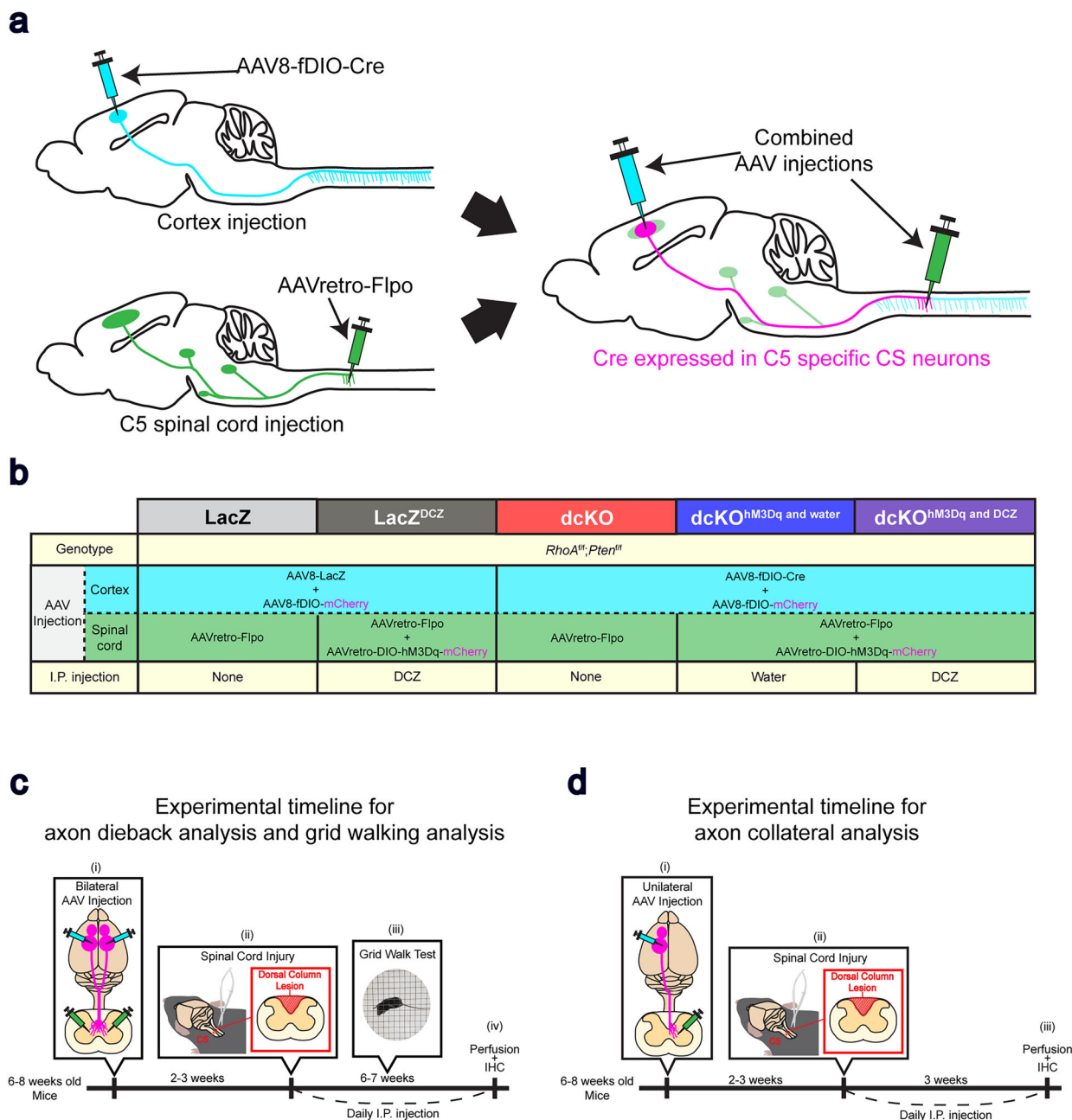
Figure 2. Experimental design. ***a***, Schematic of combinatorial AAV injections. Cortical injections of AAV8-fDIO-Cre anterogradely infects CSNs, while spinal cord injections of AAVretro-Flpo retrogradely infects multiple spinal neurons. Combination of the two injections induces the expression of Cre in C5 spinal cord-specific CSNs. Representative raw images of mCherry fluorescence are shown in Extended Data Figure 2-1. ***b***, AAV injection strategy: To delete *RhoA* and *Pten* in CSNs, AAVretro-Flpo was injected into the C5 spinal cord of *RhoA^{f/f};Pten^{f/f}* mice, followed by injection of AAV8-fDIO-Cre into the cortex. To express the excitatory DREADD receptor, hM3Dq in CSNs, AAVretro-DIO-hM3Dq-mCherry was injected into the spinal cord. To visualize CSNs, AAV8-fDIO-mCherry was also injected into the cortex of each mouse group. In LacZ and LacZ^{DCZ} cohorts, AAV8-LacZ was injected instead of AAV8-fDIO-Cre, which will result in failure of dcKO and hM3Dq expression. Intraperitoneal (i.p.) injections of DCZ were performed in LacZ^{DCZ} and dcKO^{hM3Dq and DCZ} mice, and i.p. injections of water were performed in dcKO^{hM3Dq and water} mice. ***c***, Experimental schematic and timeline for axon dieback and grid-walking analyses: (1) AAVs were bilaterally injected into the sensorimotor cortex and the C5 level of the spinal cord in 6–8-week-old *RhoA^{f/f};Pten^{f/f}* mice. Representative images of dorsal column lesion are shown in Extended Data Figure 2-2. (2) A C5 dorsal column lesion was performed 2–3 weeks after AAV injections. (3) The grid-walking test was performed weekly thereafter, followed by perfusion at 6–7 weeks postinjury. (4) Daily i.p. injections were performed during the postinjury period, and the brain and spinal cord tissues were processed for IHC analyses. ***d***, Experimental schematic and timeline for axon collateral analysis: (1) AAVs were unilaterally injected into the cortex and the C5 level of the spinal cord in 6–8-week-old *RhoA^{f/f};Pten^{f/f}* mice. (2) A C5 dorsal column lesion was performed 2–3 weeks after AAV injections. (3) Daily i.p. injections were performed during the postinjury period, followed by perfusion and IHC analyses of brains and spinal cords at 3 weeks postinjury.

DREADD, but the dcKO[hM3Dq and water] receives i.p. injections of water via a 30 G syringe which does not activate the DREADD receptor (Fig. 2b).

Two to three weeks after bilateral AAV injections, lesions were made in the C5 spinal cord, and mice were subjected to weekly grid-walking tests starting 1 week post-SCI (Fig. 2c). Starting the day after injury, DCZ was i.p. injected with a 30 G syringe into LacZ[DCZ] and dcKO[hM3Dq and DCZ] mice twice a day at a concentration of 100 µg/kg (Nagai et al., 2020; Nentwig et al., 2022). Injections continued until 42 DPI. On the days when mice were subjected to their weekly grid-walking tests, DCZ was administered twice daily after each test. To confirm whether hM3Dq was affecting behavior in the hM3Dq-expressing mice, an additional week of grid-walking tests was performed without DCZ. After the final grid-walking test, the LacZ mice and dcKO mice were transcardially perfused with 4% PFA/PBS, while the LacZ[DCZ] mice, dcKO[hM3Dq and water] mice, and dcKO[hM3Dq and DCZ] mice were administered with DCZ and perfused 2–3 h later (Fig. 2c). The brains and spinal cords were then dissected and processed for immunohistochemistry.

To quantify axon collateral projections, 6–8-week-old RhoA[f/f];Pten[f/f] mice were injected with AAVs unilaterally according to the injection plans to establish the LacZ[DCZ], dcKO, and dcKO[hM3Dq and DCZ] cohorts (Fig. 2d). SCIs were made in the C5 spinal cord 2 weeks after AAV injections. Mice were then perfused at 21 DPI, and brains and spinal cords were dissected and processed for IHC analyses (Fig. 2d).

Results

A recent study showed that modulation of extrinsic and intrinsic signaling pathways through deletion of both RhoA and Pten suppresses axon dieback after thoracic SCI (Nakamura et al., 2021). Excitation of CSNs has also been shown to promote axon sprouting following CST injury (Carmel and Martin, 2014). We examined whether combining these two approaches would augment motor recovery after cervical SCI by deleting RhoA and Pten in CSNs and chemogenetically activating those neurons in mice. We assessed the anatomical and functional effects of this combinatorial approach on CS circuit recovery after cervical SCI.

Cre recombinase induces sufficient RhoA;Pten deletion in the sensorimotor cortex

We first determined the effects of genetic deletion of RhoA and Pten in CSNs by injecting AAV-Cre into the sensorimotor cortex of RhoA[f/f];Pten[f/f] mice (Fig. 1). Coinjection of AAV1-GFP and AAV1-Cre (GFP + Cre mice, n = 4) into the sensorimotor cortex lowered the expression of both RhoA and Pten proteins compared with control mice (GFP only, n = 4; Fig. 1b). Quantitative analysis also showed significantly lower protein levels in GFP + Cre mice, indicating that Cre expression induced sufficient genetic codeletion of RhoA and Pten (Fig. 1c, Table 1).

Combination of RhoA;Pten deletion and neuronal activation suppresses axon dieback after SCI

To delete RhoA and Pten specifically in CSNs, AAV8-fDIO-Cre was injected into the sensorimotor cortex, and AAVretro-Flpo was injected into the cervical spinal cord of RhoA[f/f];Pten[f/f] mice (hereafter referred to as dcKO mice; Fig. 2).

Activation of the DREADD receptor, hM3Dq, by the addition of DCZ was evaluated by examining cFos expression in LacZ[DCZ] (n = 4), dcKO[hM3Dq and water] (n = 5), and dcKO[hM3Dq and DCZ] (n = 4) mice (Fig. 3). The number of cFos[+] and mCherry[+] CSNs in dcKO[hM3Dq and DCZ] mice was significantly higher than the other groups, indicating that Cre successfully induced the expression of the excitatory hM3Dq receptor and DCZ functioned as an actuator ligand (Fig. 3c, Table 2).

Sagittal sections of the spinal cord were examined to evaluate CS axon lengths (Fig. 4). Signal intensities of the astrocyte marker, GFAP, were elevated near the transection sites in all the groups, indicating that glial scars had formed near the lesions. In LacZ (n = 7) and LacZ[DCZ] (n = 6) mice, >50% of the mCherry[+] axons were present at 200–500 µm rostral to the lesion in the dorsal funiculus, indicating that axon dieback had occurred (Fig. 4a,c). In contrast, >50% of axons were observed at 100 µm rostral to the lesion in dcKO (n = 7), dcKO[hM3Dq and water] (n = 5), and dcKO[hM3Dq and DCZ] (n = 8) mice (Fig. 4b,d). The CST axon indices in dcKO, dcKO[hM3Dq and water], and dcKO[hM3Dq and DCZ] mice showed reduced axon dieback compared with LacZ and LacZ[DCZ] mice. To further evaluate the differences between the dcKO, dcKO[hM3Dq and water], and dcKO[hM3Dq and DCZ] mice, we measured the improvements in axon dieback suppression compared with the LacZ and LacZ[DCZ] cohorts. In both dcKO and dcKO[hM3Dq and DCZ] mice, the CST axon indices were significantly higher at 100–300 µm rostral to the lesion compared with control mice (Fig. 4f,g, Table 3a,b). These results suggest that RhoA;Pten deletion suppresses axon dieback at cervical levels. Moreover, the combination of CSN stimulation via excitatory DREADDs with RhoA;Pten deletion resulted in greater reductions in axon dieback rostral to the lesion over RhoA;Pten deletion alone (Fig. 4h, Table 3c).

Table 1. Western blot analysis statistical data

	95% confidence interval	p-value
RhoA/Tuj1	CI[low][0.5024474] CI[up][0.9392495]	0.0161
Pten/Tuj1	CI[low][0.2227772] CI[up][1.4780436]	0.0002

Table summarizing the statistical analysis of relative expression in Western blotting. Normal distribution, unpaired t test.
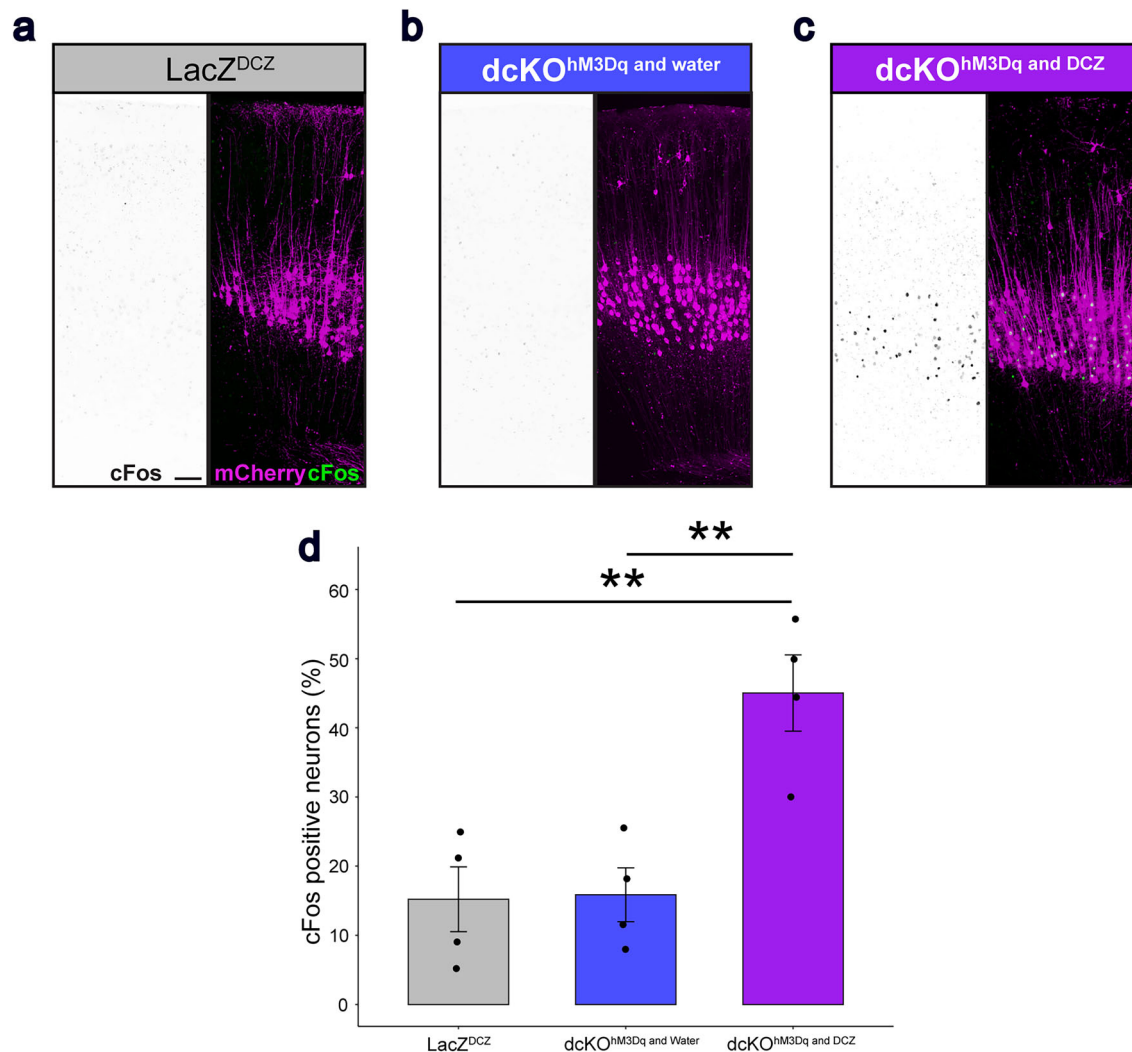
Figure 3. Neuronal stimulation by excitatory DREADDs in the sensorimotor cortex. *a–c*, Representative images of cFos staining (black on the left, green on the right) and mCherry (magenta on the right) in (*a*) LacZ^{DCZ} (*n* = 4), (*b*) dcKO$^{hM3Dq \; and \; water}$ (*n* = 5), and (*c*) dcKO$^{hM3Dq \; and \; DCZ}$ (*n* = 4) mice. Scale bar, 100 μm. *d*, Quantitative analysis of cFos$^+$ neurons in mCherry$^+$ CSNs in LacZ^{DCZ}, dcKO$^{hM3Dq \; and \; water}$, and dcKO$^{hM3Dq \; and \; DCZ}$ mice. Two-way ANOVA followed by Tukey's test. **p < 0.005. Specific data is in Table 2.

Table 2. cFos analysis statistical data

	95% confidence interval	*p*-value
Two-way ANOVA		0.0023
LacZ^{DCZ} versus dcKO$^{hM3Dq \; and \; water}$	CI^{low}[−18.09907] CI^{up}[19.3758]	0.9950
LacZ^{DCZ} versus dcKO$^{hM3Dq \; and \; DCZ}$	CI^{low}[11.08059] CI^{up}[48.55546]	0.0041
dcKO$^{hM3Dq \; and \; water}$ versus dcKO$^{hM3Dq \; and \; DCZ}$	CI^{low}[−47.91709] CI^{up}[−10.44223]	0.0047

Table summarizing the statistical analysis of cFos positive neuron percentage. Normal distribution and two-way ANOVA followed by Tukey's test.

Combination of *RhoA;Pten* deletion and excitatory DREADDs promotes forelimb motor recovery

To determine whether the combination of *RhoA;Pten* deletion in CSNs paired with neural activation can enhance motor recovery after SCI, we subjected mice to a grid-walking test (Chao et al., 2012). In this analysis of skilled behaviors, the slip rate index showed no significant differences between LacZ (*n* = 7) and dcKO mice (*n* = 9; Fig. 5*a*, Table 4a). In contrast, the dcKO with DREADD mice (dcKO$^{hM3Dq \; and \; DCZ}$; *n* = 8) showed significantly lower slip rates at 21–35 DPI in both forepaws compared with dcKO$^{hM3Dq \; and \; water}$ mice (*n* = 5; Fig. 5*b*, Table 4b). Right forepaw slip rate indices (a normalized value where each slip rate is divided by the preinjury slip rate) in the dcKO$^{hM3Dq \; and \; DCZ}$ mice were significantly lower than those of the dcKO mice at 21 DPI (Fig. 5*b*, Table 4b). When both forepaws were examined together, the slip rate was significantly lower for dcKO$^{hM3Dq \; and \; DCZ}$ mice at 21 DPI compared with LacZ^{DCZ} mice (Fig. 5*b*, Table 4b). To further evaluate the differences
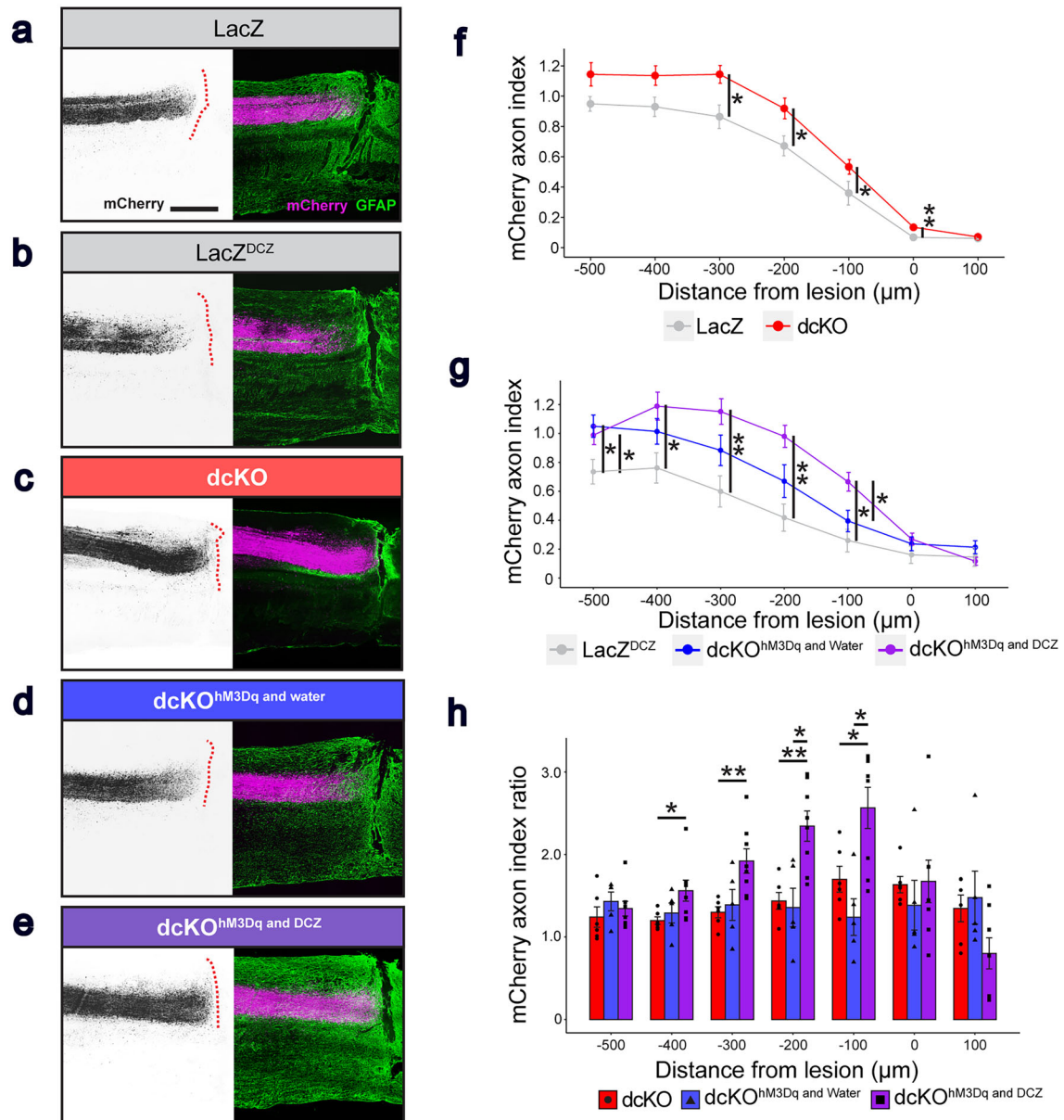
Figure 4. *RhoA;Pten* dcKO mice with DREADDs show suppression of axon dieback in the CST after SCI. *a–e*, Representative images of mCherry+ CST axons (black on the left, magenta on the right) and GFAP+ tissues (green on the right) in the cervical spinal cord in (*a*) LacZ (*n* = 6), (*b*) LacZ^DCZ (*n* = 6), (*c*) dcKO (*n* = 7), (*d*) dcKO^hM3Dq and water (*n* = 6), and (*e*) dcKO^hM3Dq and DCZ (*n* = 8) mice at 42 DPI (*a, c*) and 49 DPI (*b, d, e*). Dotted red lines indicate the borders of the GFAP+ glial scars and the GFAP− fibrotic scars. Scale bar, 500 μm. *f*, Quantification of CST axons in the dorsal funiculus in LacZ and dcKO mice. Wilcoxon rank sum exact test. *g*, Quantification of CST axons in the dorsal funiculus in LacZ^DCZ, dcKO^hM3Dq and water, and dcKO^hM3Dq and DCZ mice. Kruskal–Wallis test followed by Wilcoxon rank sum exact test. *h*, Quantification of CST axon ratios in the dorsal funiculus of dcKO and dcKO^hM3Dq and DCZ mice. Regions of interest are identified according to Extended Data Figure 4-1. Kruskal–Wallis test followed by Wilcoxon rank sum exact test. *p < 0.05, **p < 0.005. Specific data is in Table 3.

between the dcKO, dcKO^hM3Dq and water, and dcKO^hM3Dq and DCZ mice, we measured the deterioration ratio of slip rate by comparing to the LacZ and LacZ^DCZ cohorts (Fig. 5c, Table 4c). In the left forepaw, dcKO mice at 21 and 28 DPI showed significantly higher ratio. In the right forepaw, dcKO^hM3Dq and DCZ mice at 21 and 35 DPI showed significantly lower ratio. In both forepaws, dcKO^hM3Dq and DCZ mice at 21 DPI showed significantly lower ratio. These results indicate that *RhoA;Pten* deletion in CSNs alone has limited effect on forelimb motor recovery; however, the addition of excitatory DREADDs significantly enhances forelimb motor functioning after SCI.

Combination of *RhoA;Pten* deletion and excitatory DREADDs promotes formation of presynaptic boutons after SCI

Activation of CSNs by excitatory DREADDs at 21 DPI was evaluated by examining cFos expression in dcKO^hM3Dq and DCZ mice (*n* = 3) and their controls (LacZ^DCZ, *n* = 3; Fig. 6a, Table 5a). mCherry+ CSNs in dcKO^hM3Dq and DCZ mice showed

Table 3. Axon dieback analysis statistical data

a. Data summary of Figure 4f

Distance from lesion (μm)	−500	−400	−300	−200	−100	0	100
LacZ versus dcKO p-value	0.1255	0.0519	0.0303	0.0087	0.0087	0.0043	0.3290

b. Data summary of Figure 4g

Distance from lesion (μm)	−500	−400	−300	−200	−100	0	100
Kruskal–Wallis p-value	0.0253	0.0241	0.0123	0.0057	0.0129	0.0948	0.1346
LacZ^{DCZ} versus dcKO$^{hM3Dq\ and\ water}$ p-value	0.0170	0.1770	0.1255	0.1255	0.1770		
LacZ^{DCZ} versus dcKO$^{hM3Dq\ and\ DCZ}$ p-value	0.0290	0.0080	0.0047	0.0027	0.0130		
dcKO$^{hM3Dq\ and\ water}$ versus dcKO$^{hM3Dq\ and\ DCZ}$ p-value	0.5240	0.2220	0.1274	0.0451	0.0300		

c. Data summary of Figure 4h

Distance from lesion (μm)	−500	−400	−300	−200	−100	0	100
Kruskal–Wallis p-value	0.3658	0.0386	0.0102	0.0073	0.0106	0.3595	0.0825
dcKO versus dcKO$^{hM3Dq\ and\ water}$ p-value		0.4290	0.7922	0.9307	0.0820		
dcKO versus dcKO$^{hM3Dq\ and\ DCZ}$ p-value		0.1710	0.0653	0.0186	0.0110		
dcKO$^{hM3Dq\ and\ water}$ versus dcKO$^{hM3Dq\ and\ DCZ}$ p-value		0.0130	0.0013	0.0027	0.0430		

Table summarizing the statistical analysis of mCherry axon index and the ratio. Non-normal distribution and Wilcoxon rank sum exact test (a). Non-normal distribution and Kruskal–Wallis test followed by Wilcoxon rank sum exact test (b). Non-normal distribution and Kruskal–Wallis test followed by Wilcoxon rank sum exact test (c).

greater cFos expression than CSNs in LacZ^{DCZ} mice, indicating that excitatory DREADDs were induced successfully to activate CSNs.

We then examined axon collaterals in the spinal gray matter (Fig. 6b). In dcKO$^{hM3Dq\ and\ DCZ}$ mice (n = 7), intensities of CST collaterals in the gray matter did not differ significantly from those in LacZ^{DCZ} (n = 4) and dcKO (n = 4) mice (Fig. 6c, Table 5b). However, when the gray matter was separated into four regions (ipsidorsal, contradorsal, ipsiventral, and contraventral areas; Fig. 6d, Table 5c), the contradorsal area at 200 μm rostral to the lesion site showed significantly greater axon collaterals in the two-pronged treatment cohort (dcKO$^{hM3Dq\ and\ DCZ}$) compared with the singular treatment group involving only genetic deletions (dcKO).

Lastly, we evaluated the number of presynaptic boutons in the spinal gray matter. The bouton indices (the amount of presynaptic structure of CSNs) in dcKO (n = 4) and dcKO$^{hM3Dq\ and\ DCZ}$ (n = 7) mice were significantly higher than controls (LacZ^{DCZ}, n = 4) at the lesion and caudal to the lesion site (Fig. 6e,f, Table 5d). At 50 μm caudal to the lesion, dcKO$^{hM3Dq\ and\ DCZ}$ mice showed significantly higher values than dcKO mice, indicating that neural stimulation through DREADDs promotes the formation of presynaptic boutons between CSNs and spinal interneurons in the spinal gray matter after SCI.

Discussion

Rehabilitation following SCI involves both neural regeneration and circuit formation in the affected body regions. A previous study showed that *RhoA;Pten* co-deletion promotes sprouting of CSNs after SCI but was insufficient to regain motor function (Nakamura et al., 2021). Other studies have shown that axon sprouting promoted by neuronal stimulation can lead to functional recovery in mice (Carmel and Martin, 2014; Brommer et al., 2021; Squair et al., 2021; Van Steenbergen et al., 2023). We hypothesized that a combinatorial approach involving both neuronal stimulation and *RhoA;Pten* deletion enhances axon growth and leads to motor recovery after SCI. In this study, we combined genetic deletion of *RhoA* and *Pten* in CSNs with chemogenetic stimulation of CSNs via excitatory DREADDs and examined the levels of axon regrowth and forelimb motor function after cervical SCI. Our results revealed that the synergistic effects of genetic deletion of *RhoA;Pten* and CSN stimulation limited axon dieback and promoted presynaptic growth in CSN axons at and below the site of injury. Furthermore, this combinatorial treatment accelerated the recovery of skilled locomotor behaviors after SCI.

An earlier study showed that mice lacking *RhoA* and *Pten* exhibited less axon dieback than controls (Nakamura et al., 2021). Hindlimb motor function was not restored in those mice (Nakamura et al., 2021). Similarly, in our current study focused on cervical SCIs, we found that genetic deletion of *RhoA* and *Pten* alone did not induce motor recovery in mice. However, when excitatory DREADDs that stimulate CSNs were combined with *RhoA;Pten* deletion, axon dieback was reduced to a greater extent than that in mice that had only undergone *RhoA;Pten* deletion. It is worth noting that our quantification of axon dieback relied on fluorescence intensity as a surrogate measure for axon number, which may be influenced by variations in viral injection efficiency or experimental conditions. Although the excitatory DREADDs and *RhoA;Pten* deletion promoted regrowth of injured CS axons, motor function was not fully restored. Bridging the lesion and keeping neurons in an immature state with neural stem cell (NSC) grafts (Kadoya et al., 2016; Poplawski et al., 2020; Zheng and Tuszynski, 2023), or neutralizing extracellular inhibitors at the lesion site (Houle et al., 2006;
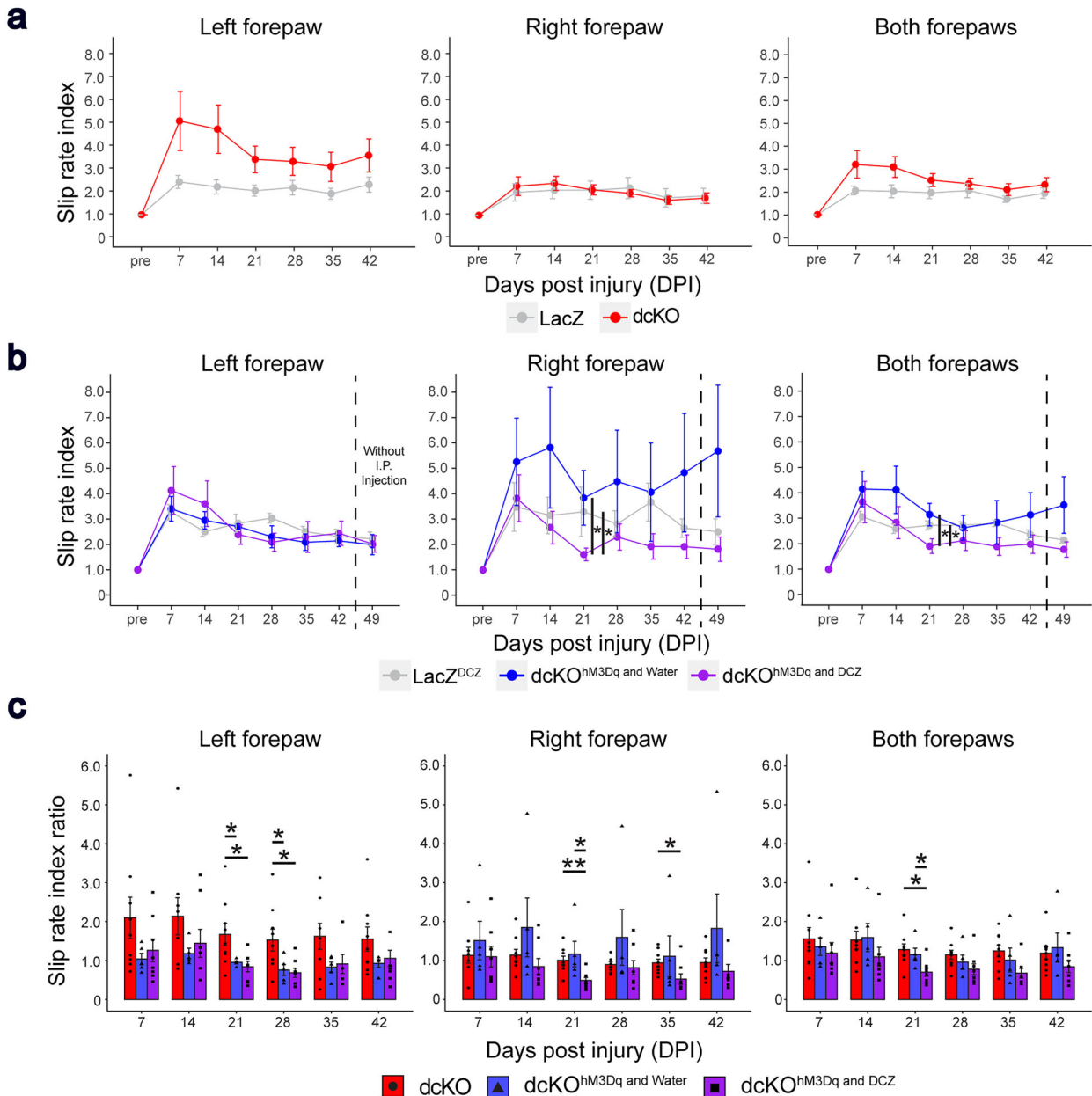
Figure 5. The combination of *RhoA;Pten* deletion and neuronal stimulation enhances motor recovery after SCI. ***a***, Forelimb slip rate indices of the left (left panels), right (middle panels), and both forepaws (right panels) in LacZ ($n = 7$) and dcKO mice ($n = 9$) on the grid-walking test. Wilcoxon rank sum exact test. ***b***, Forelimb slip rate indices of the left (left panels), right (middle panels), and both forepaws (right panels) in LacZ[DCZ] ($n = 7$), dcKO[hM3Dq and water] ($n = 6$), and dcKO[hM3Dq and DCZ] mice ($n = 8$) on the grid-walking test. Dotted lines indicate when DCZ administration was stopped. Kruskal–Wallis test followed by Wilcoxon rank sum exact test. ***c***, Slip ratios of the left (left panel), right (middle panel), and both forepaws (right panel) in dcKO, dcKO[hM3Dq and water], and dcKO[hM3Dq and DCZ] mice. Kruskal–Wallis test followed by Wilcoxon rank sum exact test. *$p < 0.05$, **$p < 0.005$. Specific data is in Table 4.

García-Alías et al., 2009; Zheng and Tuszynski, 2023), may promote greater CS axonal growth in the spinal cord. These additional treatments may be required as part of a multipronged strategy to enhance functional recovery.

Following dorsal hemisection injuries at thoracic levels in in which the CST is transected, mice lacking *RhoA* and *Pten* exhibit less axon dieback, but are still impaired in hindlimb motor control (Nakamura et al., 2021). Given the critical role that the CST plays in voluntary skilled behaviors of the forelimb, we examined forelimb motor behaviors in dcKO and dcKO with DREADD (dcKO[hM3Dq and water] and dcKO[hM3Dq and DCZ]) mice in a grid-walking test (Schaar et al., 2010; Chao et al., 2012). The dcKO[hM3Dq and DCZ] mice showed faster motor function recovery at 21 DPI compared with dcKO and dcKO[hM3Dq and water] mice. Although this combinatorial approach promoted early motor recovery after SCI, full motor function was never achieved. Full restoration of motor behaviors may have been hindered for several reasons. First, the limited axon regrowth observed following SCI may be insufficient for regaining preinjury levels of motor control. Other strategies, such as NSC

Table 4. Grid-walking analysis statistical data

a. Data summary of Fig.5a

	Days post injury(DPI)	7	14	21	28	35	42
Left forepaw	LacZ vs dcKO p-value	0.0800	0.1400	0.1000	0.2400	0.2200	0.2900
Right forepaw	LacZ vs dcKO p-value	0.7900	0.7900	0.8700	0.7900	0.7100	0.9200
Both forepaws	LacZ vs dcKO p-value	0.1400	0.0800	0.2900	0.0920	0.2400	0.6300

b. Data summary of Fig.5b

	Days post injury(DPI)	7	14	21	28	35	42	49
Left forepaw	Kruskal-Wallis p-value	0.9685	0.6742	0.6694	0.0989	0.3991	0.9560	0.8426
	LacZ^{DCZ} vs dcKO$^{hM3Dq\ and\ Water}$ p-value							
	LacZ^{DCZ} vs dcKO$^{hM3Dq\ and\ DCZ}$ p-value							
	dcKO$^{hM3Dq\ and\ Water}$ vs dcKO$^{hM3Dq\ and\ DCZ}$ p-value							
Right forepaw	Kruskal-Wallis p-value	0.2875	0.1986	0.0199	0.4315	0.0652	0.1036	0.0650
	LacZ^{DCZ} vs dcKO$^{hM3Dq\ and\ Water}$ p-value			0.4600				
	LacZ^{DCZ} vs dcKO$^{hM3Dq\ and\ DCZ}$ p-value			0.0180				
	dcKO$^{hM3Dq\ and\ Water}$ vs dcKO$^{hM3Dq\ and\ DCZ}$ p-value			0.0370				
Both forepaws	Kruskal-Wallis p-value	0.4619	0.1782	0.0379	0.1115	0.0610	0.3065	0.1475
	LacZ^{DCZ} vs dcKO$^{hM3Dq\ and\ Water}$ p-value			0.8070				
	LacZ^{DCZ} vs dcKO$^{hM3Dq\ and\ DCZ}$ p-value			0.0450				
	dcKO$^{hM3Dq\ and\ Water}$ vs dcKO$^{hM3Dq\ and\ DCZ}$ p-value			0.0320				

c. Data summary of Fig.5c

	Days post injury(DPI)	7	14	21	28	35	42
Left forepaw	Kruskal-Wallis p-value	0.2061	0.5409	0.0210	0.0196	0.2479	0.4169
	dcKO vs dcKO$^{hM3Dq\ and\ Water}$ p-value			0.0330	0.0450		
	dcKO vs dcKO$^{hM3Dq\ and\ DCZ}$ p-value			1.0000	0.6060		
	dcKO$^{hM3Dq\ and\ Water}$ vs dcKO$^{hM3Dq\ and\ DCZ}$ p-value			0.0180	0.0140		
Right forepaw	Kruskal-Wallis p-value	0.6629	0.1156	0.0049	0.3857	0.0449	0.1659
	dcKO vs dcKO$^{hM3Dq\ and\ Water}$ p-value			0.7888		0.3500	
	dcKO vs dcKO$^{hM3Dq\ and\ DCZ}$ p-value			0.0184		0.1400	
	dcKO$^{hM3Dq\ and\ Water}$ vs dcKO$^{hM3Dq\ and\ DCZ}$ p-value			0.0032		0.0230	
Both forepaws	Kruskal-Wallis p-value	0.2971	0.1050	0.0165	0.0594	0.0620	0.1536
	dcKO vs dcKO$^{hM3Dq\ and\ Water}$ p-value			0.4376			
	dcKO vs dcKO$^{hM3Dq\ and\ DCZ}$ p-value			0.0451			
	dcKO$^{hM3Dq\ and\ Water}$ vs dcKO$^{hM3Dq\ and\ DCZ}$ p-value			0.0079			

Table summarizing the statistical analysis of slip rate index and the ratio. Non-normal distribution and Wilcoxon rank sum exact test (a). Non-normal distribution and Kruskal–Wallis test followed by Wilcoxon rank sum exact test (b). Non-normal distribution and Kruskal–Wallis test followed by Wilcoxon rank sum exact test (c).

grafts (Kadoya et al., 2016; Poplawski et al., 2020; Zheng and Tuszynski, 2023), rehabilitation (van den Brand et al., 2012; Wang et al., 2023), or chondroitinase treatment with peripheral nerve grafts (Alilain et al., 2011; Lee et al., 2013), might further enhance motor recovery if added to the treatment regimen. A second possible explanation is that other circuits in addition to the CST, such as other descending and ascending sensory fibers, may also require restoration to regain full functionality. Finally, continuous administration of hM3Dq may result in its downregulation, which would lower the activation of CSNs (Roth, 2016). Though complete motor recovery was not observed, this study shows at least partial restoration of skilled movements following SCI.

To determine how this partial motor recovery was achieved, we examined presynaptic bouton formation in dcKO and dcKO mice with DREADDs (dcKO$^{hM3Dq\ and\ DCZ}$). The previous study showed that *RhoA;Pten* deletion in CSNs promotes axon sprouting after SCI at thoracic levels and that synapse formation may be increased in these mice (Nakamura et al., 2021). In the present study, however, axon sprouting was absent in dcKO mice after cervical SCI, suggesting that circuit rewiring mechanisms may differ in the cervical and thoracic spinal regions. Interestingly, the addition of excitatory DREADDs that stimulate CSNs in dcKO mice caused an increase in presynaptic boutons in CST axons proximal and caudal to the cervical spinal cord lesion. Several studies have shown that excitatory DREADDs can promote presynaptic connections, while inhibitory DREADDs decrease the total number of boutons following SCI (Bradley et al., 2019; Gao et al., 2021). Therefore, presynaptic formation in CSNs may be induced by the combination of *RhoA* and *Pten* deletion coupled with neuronal activation after SCI, and this may synergistically promote motor recovery. Future motor circuit analyses using pseudorabies virus assays or electromyography after the cortical stimulation will be necessary to characterize the different stages of circuit repair promoted by this two-pronged approach.
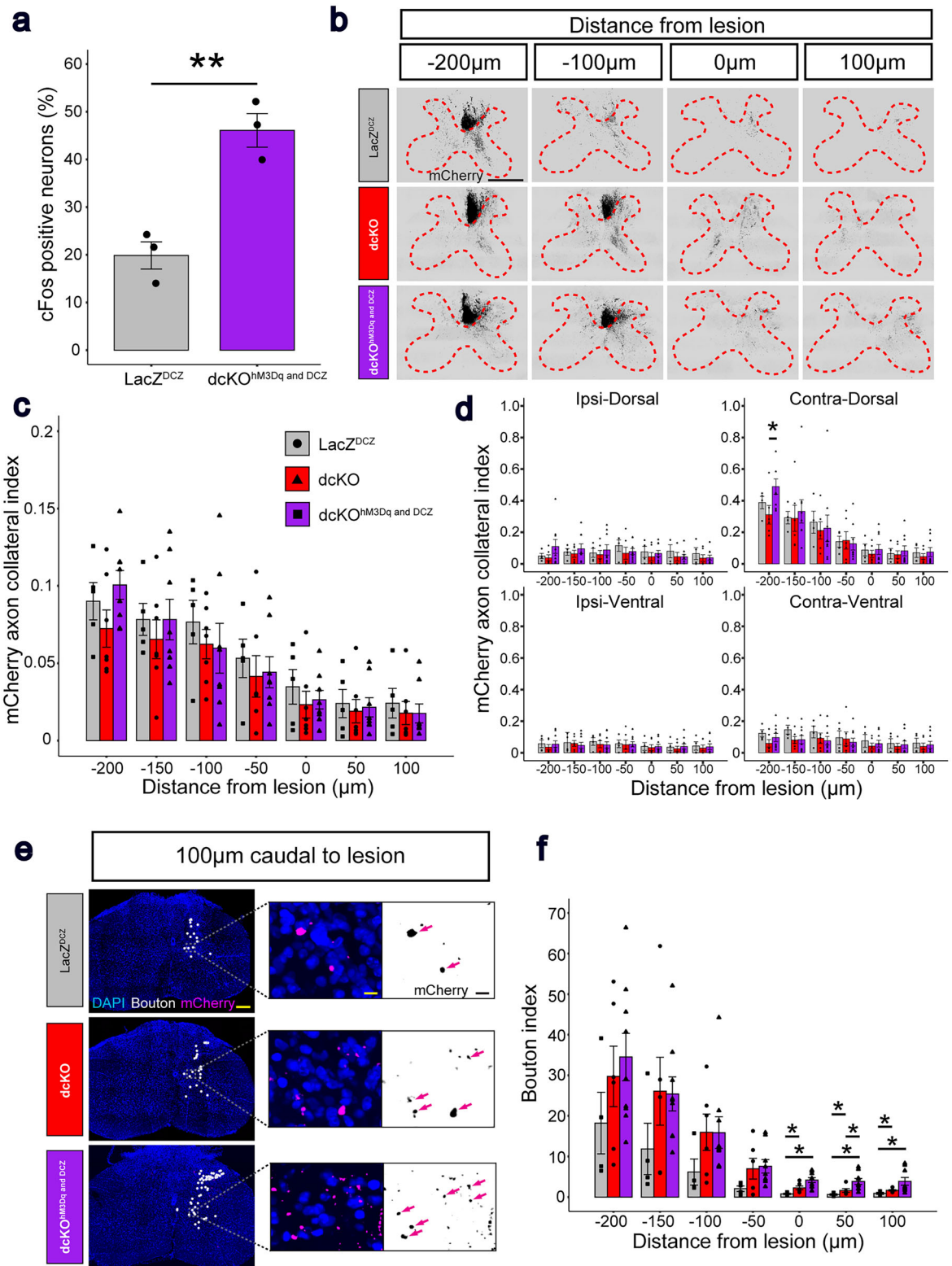
Figure 6. The combination of *RhoA* and *Pten* deletion and neuronal stimulation promotes synaptogenesis in the CST after SCI. *a*, Quantitative analysis of cFos^{+} neurons in mCherry[+] CSNs in LacZ[DCZ] (*n* = 3) and dcKO[hM3Dq and DCZ] mice (*n* = 3). Unpaired *t* test. *b*, Representative images of mCherry[+] CST axons (black) in the cervical spinal cord in LacZ[DCZ] (top), dcKO (middle), and dcKO[hM3Dq and DCZ] (bottom) mice at 21 DPI. Dotted red lines indicate the borders between the white and gray matter. Scale bar, 500 μm. *c*, Quantification of mCherry[+] CST axon collateral indices in the gray matter. Kruskal–Wallis test followed by Wilcoxon rank sum exact test. *d*, Quantification of mCherry[+] CST axon collateral indices in four regions: ipsidorsal (left top), ipsiventral (right bottom), contradorsal (right top), and contraventral (right bottom) in LacZ[DCZ] (*n* = 4), dcKO (*n* = 4), and dcKO[hM3Dq and DCZ] mice (*n* = 7). Kruskal–Wallis test followed by Wilcoxon rank sum exact test. *e*, Representative images of mCherry[+] (magenta on left and center, black on right), presynaptic boutons

Table 5. Axon collateral and bouton analysis statistical data

a. Data summary of Figure 6a

	95% confidence interval		p-value
LacZ^{DCZ} versus dcKO$^{hM3Dq\ and\ DCZ}$	CI^{low}[13.67379]	CI^{up}[38.79031]	0.004396

b. Data summary of Figure 6c

Days postinjury (DPI)	−200	−150	−100	−50	0	50	100
Kruskal–Wallis p-value	0.5392	0.8333	0.8767	0.9597	0.9155	0.9082	0.9803
LacZ^{DCZ} versus dcKO p-value							
LacZ^{DCZ} versus dcKO$^{hM3Dq\ and\ DCZ}$ p-value							
dcKO versus dcKO$^{hM3Dq\ and\ DCZ}$ p-value							

c. Data summary of Figure 6d

	Days postinjury (DPI)	−200	−150	−100	−50	0	50	100
Ipsidorsal	Kruskal–Wallis p-value	0.1965	0.762	0.3693	0.2158	0.26	0.281	0.2424
	LacZ^{DCZ} versus dcKO p-value							
	LacZ^{DCZ} versus dcKO$^{hM3Dq\ and\ DCZ}$ p-value							
	dcKO versus dcKO$^{hM3Dq\ and\ DCZ}$ p-value							
Contradorsal	Kruskal–Wallis p-value	0.0294	0.8359	0.7621	0.7317	0.5421	0.4992	0.2434
	LacZ^{DCZ} versus dcKO p-value	0.2401						
	LacZ^{DCZ} versus dcKO$^{hM3Dq\ and\ DCZ}$ p-value	0.3159						
	dcKO versus dcKO$^{hM3Dq\ and\ DCZ}$ p-value	0.0292						
Ipsiventral	Kruskal–Wallis p-value	0.2063	0.4207	0.5025	0.541	0.179	0.1933	0.2404
	LacZ^{DCZ} versus dcKO p-value							
	LacZ^{DCZ} versus dcKO$^{hM3Dq\ and\ DCZ}$ p-value							
	dcKO versus dcKO$^{hM3Dq\ and\ DCZ}$ p-value							
Contraventral	Kruskal–Wallis p-value	0.2763	0.3678	0.4795	0.7963	0.3071	0.4042	0.3393
	LacZ^{DCZ} versus dcKO p-value							
	LacZ^{DCZ} versus dcKO$^{hM3Dq\ and\ DCZ}$ p-value							
	dcKO versus dcKO$^{hM3Dq\ and\ DCZ}$ p-value							

d. Data summary of Figure 6f

Days postinjury (DPI)	−200	−150	−100	−50	0	50	100
Kruskal–Wallis p-value	0.228	0.3204	0.2014	0.133	0.0066	0.005	0.0279
LacZ^{DCZ} versus dcKO p-value					0.0252	0.0428	0.0428
LacZ^{DCZ} versus dcKO$^{hM3Dq\ and\ DCZ}$ p-value					0.0069	0.0069	0.0168
dcKO versus dcKO$^{hM3Dq\ and\ DCZ}$ p-value					0.0518	0.0292	0.0518

Table summarizing the statistical analysis of cFos positive neuron percentage, axon collateral index, and bouton index. Normal distribution and unpaired t test (a). Non-normal distribution and Kruskal–Wallis test followed by Wilcoxon rank sum exact test (b). Non-normal distribution and Kruskal–Wallis test followed by Wilcoxon rank sum exact test (c). Non-normal distribution and Kruskal–Wallis test followed by Wilcoxon rank sum exact test (d).

Taken together, our results suggest that the effects of *RhoA*;*Pten* deletion combined with neuronal activation of CSNs may be a useful therapeutic approach to promote axonal growth and motor recovery after SCI. The gains in motor function observed with this two-pronged method open the door to other multifaceted treatment regimens that may elicit greater recovery of movement and functioning after SCI. Future treatment paradigms could involve a mix-and-match model tailored to the specific type and location of a SCI to deliver maximum therapeutic benefits.

Data Availability

The datasets used and analyzed during the current study are available from the corresponding author upon reasonable request.

←

(white dots, analyzed by IMARIS on left and center), and DAPI (blue, on left and center) within the gray matter in LazZ^{DCZ} (top row), dcKO (middle row), and dcKO$^{hM3Dq\ and\ DCZ}$ (bottom row) mice at 21 DPI. Magenta arrows indicate boutons. Scale bars, 200 μm (left) and 10 μm (right). *f*, Quantification of boutons in the gray matter in LacZ^{DCZ} ($n = 4$), dcKO ($n = 4$), and dcKO$^{hM3Dq\ and\ DCZ}$ mice ($n = 7$). Kruskal–Wallis test followed by Wilcoxon rank sum exact test. *$p < 0.05$, **$p < 0.005$. Specific data is in Table 5.

References

Alilain WJ, Horn KP, Hu H, Dick TE, Silver J (2011) Functional regeneration of respiratory pathways after spinal cord injury. Nature 475:196–200.

Blackmore MG, Wang Z, Lerch JK, Motti D, Zhang YP, Shields CB, LeeJK, Goldberg JL, Lemmon VP, Bixby JL (2012) Krüppel-like factor 7 engineered for transcriptional activation promotes axon regeneration in the adult corticospinal tract. Proc Natl Acad Sci U S A 109:7517–7522.

Boato F, et al. (2010) C3 peptide enhances recovery from spinal cord injury by improved regenerative growth of descending fiber tracts. J Cell Sci 123:1652–1662.

Bradley PM, Denecke CK, Aljovic A, Schmalz A, Kerschensteiner M, Bareyre FM (2019) Corticospinal circuit remodeling after central nervous system injury is dependent on neuronal activity. J Exp Med 216:2503–2514.

Brommer B, et al. (2021) Improving hindlimb locomotor function by non-invasive AAV-mediated manipulations of propriospinal neurons in mice with complete spinal cord injury. Nat Commun 12:781.

Carmel JB, Martin JH (2014) Motor cortex electrical stimulation augments sprouting of the corticospinal tract and promotes recovery of motor function. Front Integr Neurosci 8:51.

Chao OY, Pum ME, Li J-S, Huston JP (2012) The grid-walking test: assessment of sensorimotor deficits after moderate or severe dopamine depletion by 6-hydroxydopamine lesions in the dorsal striatum and medial forebrain bundle. Neuroscience 202:318–325.

Chauhan BK, Lou M, Zheng Y, Lang RA (2011) Balanced Rac1 and RhoA activities regulate cell shape and drive invagination morphogenesis in epithelia. Proc Natl Acad Sci U S A 108:18289–18294.

Duffy P, Andre S, Antonio S, Sigworth J, Narumiya S, Cafferty WBJ, Strittmatter SM (2009) Rho-associated kinase II (ROCKII) limits axonal growth after trauma within the adult mouse spinal cord. J Neurosci 29:15266–15276.

Fenno LE, et al. (2014) Targeting cells with single vectors using multiple-feature Boolean logic. Nat Methods 11:763–772.

Fournier AE, Takizawa BT, Strittmatter SM (2003) Rho kinase inhibition enhances axonal regeneration in the injured CNS. J Neurosci 23:1416–1423.

Fujita Y, Yamashita T (2014) Axon growth inhibition by RhoA/ROCK in the central nervous system. Front Neurosci 8:338.

Gao Z, Yang Y, Feng Z, Li X, Min C, Zhu Z, Song H, Hu Y, Wang Y, He X (2021) Chemogenetic stimulation of proprioceptors remodels lumbar interneuron excitability and promotes motor recovery after SCI. Mol Ther 29:2483–2498.

García-Alías G, Barkhuysen S, Buckle M, Fawcett JW (2009) Chondroitinase ABC treatment opens a window of opportunity for task-specific rehabilitation. Nat Neurosci 12:1145–1151.

Hollis ER 2nd, et al. (2016) Ryk controls remapping of motor cortex during functional recovery after spinal cord injury. Nat Neurosci 19:697–705.

Houle JD, Tom VJ, Mayes D, Wagoner G, Phillips N, Silver J (2006) Combining an autologous peripheral nervous system "bridge" and matrix modification by chondroitinase allows robust, functional regeneration beyond a hemisection lesion of the adult rat spinal cord. J Neurosci 26:7405–7415.

Kadoya K, et al. (2016) Spinal cord reconstitution with homologous neural grafts enables robust corticospinal regeneration. Nat Med 22:479–487.

Katayama K-I, Melendez J, Baumann JM, Leslie JR, Chauhan BK, Nemkul N, Lang RA, Kuan C-Y, Zheng Y, Yoshida Y (2011) Loss of RhoA in neural progenitor cells causes the disruption of adherens junctions and hyperproliferation. Proc Natl Acad Sci U S A 108:7607–7612.

Krashes MJ, Koda S, Ye C, Rogan SC, Adams AC, Cusher DS, Maratos-Flier E, Roth BL, Lowell BB (2011) Rapid, reversible activation of AgRP neurons drives feeding behavior in mice. J Clin Invest 121:1424–1428.

Lee Y-S, Lin C-Y, Jiang H-H, Depaul M, Lin VW, Silver J (2013) Nerve regeneration restores supraspinal control of bladder function after complete spinal cord injury. J Neurosci 33:10591–10606.

Lesche R, Groszer M, Gao J, Wang Y, Messing A, Sun H, Liu X, Wu H (2002) Cre/loxP-mediated inactivation of the murine Pten tumor suppressor gene. Genesis 32:148–149.

Liu K, et al. (2010) PTEN deletion enhances the regenerative ability of adult corticospinal neurons. Nat Neurosci 13:1075–1081.

Melendez J, Stengel K, Zhou X, Chauhan BK, Debidda M, Andreassen P, Lang RA, Zheng Y (2011) Rhoa GTPase is dispensable for actomyosin regulation but is essential for mitosis in primary mouse embryonic fibroblasts. J Biol Chem 286:15132–15137.

Nagai Y, et al. (2020) Deschlorocozapine, a potent and selective chemogenetic actuator enables rapid neuronal and behavioral modulations in mice and monkeys. Nat Neurosci 23:1157–1167.

Nakamura Y, Ueno M, Niehaus JK, Lang RA, Zheng Y, Yoshida Y (2021) Modulation of both intrinsic and extrinsic factors additively promotes rewiring of corticospinal circuits after spinal cord injury. J Neurosci 41:10247–10260.

Nentwig TB, Obray JD, Vaughan DT, Chandler LJ (2022) Behavioral and slice electrophysiological assessment of DREADD ligand, deschlorocozapine (DCZ) in rats. Sci Rep 12:6595.

Nicola FDC, Hua I, Levine AJ (2022) Intersectional genetic tools to study skilled reaching in mice. Exp Neurol 347:113879.

Oudega M, Perez MA (2012) Corticospinal reorganization after spinal cord injury. J Physiol 590:3647–3663.

Poplawski GHD, et al. (2020) Injured adult neurons regress to an embryonic transcriptional growth state. Nature 581:77–82.

Porter R, Lemon R (1993) *Corticospinal function and voluntary movement*. Oxford, UK: Clarendon Press.

Roth BL (2016) DREADDs for neuroscientists. Neuron 89:683–694.

Schaar KL, Brenneman MM, Savitz SI (2010) Functional assessments in the rodent stroke model. Exp Transl Stroke Med 2:13.

Schneeberger M, et al. (2019) Regulation of energy expenditure by brainstem GABA neurons. Cell 178:672–685.e12.

Squair JW, Gautier M, Sofroniew MV, Courtine G, Anderson MA (2021) Engineering spinal cord repair. Curr Opin Biotechnol 72:48–53.

van den Brand R, et al. (2012) Restoring voluntary control of locomotion after paralyzing spinal cord injury. Science 336:1182–1185.

Van Steenbergen V, Burattini L, Trumpp M, Fourneau J, Aljovic A, Chahin M, Oh H, D'Ambra M, Bareyre FM (2023) Coordinated neurostimulation promotes circuit rewiring and unlocks recovery after spinal cord injury. J Exp Med 220:e20220615.

Wang X, et al. (2017) Deconstruction of corticospinal circuits for goal-directed motor skills. Cell 171:440–455.e14.

Wang Y, Luo H, Liu Y, Yang C, Yin Y, Tan B (2023) Multimodal rehabilitation promotes axonal sprouting and functional recovery in a murine model of spinal cord injury (SCI). Neurosci Lett 795:137029.

Wang Z, Reynolds A, Kirry A, Nienhaus C, Blackmore MG (2015) Overexpression of Sox11 promotes corticospinal tract regeneration after spinal injury while interfering with functional recovery. J Neurosci 35:3139–3145.

Yang L, Martin JH (2023) Effects of motor cortex neuromodulation on the specificity of corticospinal tract spinal axon outgrowth and targeting in rats. Brain Stimul 16:759–771.

Zhang J, Yang D, Huang H, Sun Y, Hu Y (2018) Coordination of necessary and permissive signals by PTEN inhibition for CNS axon regeneration. Front Neurosci 12:558.

Zheng B, Tuszynski MH (2023) Regulation of axonal regeneration after mammalian spinal cord injury. Nat Rev Mol Cell Biol 24:396–413.